The Astrophysical Journal Letters, 939:L15 (5pp), 2022 November 1 https://doi.org/10.3847/2041-8213/ac9668

Searching for the Signal of a Primordial Black Hole from CMB Lensing and γ-Ray Emissions

Xiu-Hui Tan[1], Yang-Jie Yan[1], Taotao Qiu[2], and Jun-Qing Xia[1,3]
[1] Department of Astronomy, Beijing Normal University, Beijing 100875, People's Republic of China; xiajq@bnu.edu.cn
[2] School of Physics, Huazhong University of Science and Technology, Wuhan, 430074, People's Republic of China; qiutt@hust.edu.cn
[3] Institute for Frontiers in Astronomy and Astrophysics, Beijing Normal University, Beijing 100875, People's Republic of China
Received 2022 July 29; revised 2022 September 29; accepted 2022 September 29; published 2022 October 28

Abstract

In this letter, we search for the signal of primordial black holes (PBHs) by correlating the γ-ray emissions in the MeV energy band produced by the Hawking evaporation and the lensing effect of the cosmic microwave background (CMB). We use the conservative case of the astrophysical model as much as possible in the calculations, since the potential astrophysical origins dominate the observed emission in the MeV energy band. By carefully discussing the appropriate energy bands corresponding to different PBH masses, it is worth expecting a tight constraint on the fraction of the Schwarzschild PBHs in the mass range of 10^{16}–5×10^{17} g by simulations of the sensitivity of the future CMB-S4 project and the γ-ray telescope e-ASTROGAM. Furthermore, we also consider the PBH model with spins and find that the constraining ability of the PBH fraction from the correlation between CMB lensing and γ-ray emissions can be improved by another order of magnitude, which could importantly fill the gaps with PBH fraction limits in the mass range of 5×10^{17}–2×10^{18} g.

Unified Astronomy Thesaurus concepts: Primordial black holes (1292); Cosmic microwave background radiation (322); Gamma-ray sources (633)

1. Introduction

Dark matter (DM) as one of the main components of the universe has been confirmed by numerous astrophysical and cosmological observations (Aghanim et al. 2020; Pardo & Spergel 2020). However, there are still many debates on the candidates of DM that need further investigation (Boveia & Doglioni 2018). Since primordial black holes (PBHs) are the rare well-motivated DM model that does not require physics beyond the standard model (Carr et al. 2016), viewing the PBHs as the DM has been reemphasized recently, after the first detection of the binary black hole merger by the LIGO-Virgo collaboration (LIGO Scientific et al. 2016).

Generally, PBHs are formed in the very early part of the cosmic radiation–dominated period, from the Planck time to the postinflation era (Hawking 1971). There are many mechanisms to its formation in the literature. The main mechanism for generating PBHs is that the original perturbation reenters the event horizon, becomes the overdensity region to collapse, and finally merges to form PBHs. However, regardless of the formation mechanism by which PBHs are made, they will radiate by Hawking evaporation (HE; Hawking 1975).

Based on the HE theory, PBHs can directly emit various standard model particles, such as photons, neutrinos, electrons/positrons, etc. When these primary particles propagate in the universe, it is possible to radiate secondary particles through decay or hadronization processes. If the number of PBHs is sufficient, this emission has the potential to contribute to the observable background radiation.

Due to the relationship between the rate of HE and the mass of PBHs, PBHs with a mass greater than 5×10^{14} g can survive until today and contribute as part of DM (MacGibbon et al. 2008). Thanks to their rich phenomenological properties, nonrotational PBHs with masses $M_{\rm PBH}$ between 5×10^{14} and 2×10^{17} g have been extensively studied, and numerous observational data can be used to strictly constrain the key parameter of the PBHs, the fraction $f_{\rm PBH} \equiv \Omega_{\rm PBH}/\Omega_{\rm DM}$. However, the limit of $f_{\rm PBH}$ still leaves a wide window for further exploration for PBH masses in the range of 2×10^{17}–10^{23} g. Some recent works on the upcoming AMEGO (McEnery et al. 2019) and e-ASTROGAM (e-ASTROGAM et al. 2018) observational projects studied PBHs with mass up to $\sim 10^{18}$ g by searching for the evaporating signature over the Galactic and extragalactic γ-ray background (Carr et al. 2010, 2021; Coogan et al. 2021; Ray et al. 2021; Auffinger 2022). Ballesteros et al. (2020) estimated the sensitivity to the PBH abundance of a future X-ray experiment as capable of distinguishing the contribution to diffuse background in the MeV range; isotropic X-ray and soft γ-ray background are proved as an extremely promising target by Iguaz et al. (2021); 21 cm absorption signal from the EDGES experiment (Ptak et al. 2007; Saha & Laha 2022; Mittal et al. 2022); the Galactic 511 keV line (DeRocco & Graham 2019) and inner galaxy (Berteaud et al. 2022) by INTEGRAL satellite have placed strong constraints on the fraction of DM, respectively.

In our consideration, if we regard PBHs as a kind of DM formed by the gravitational interaction, the γ-ray emissions with a certain energy range radiated by the HE can trace the spatial distribution of PBHs in the large-scale structure of the universe. On the other hand, there is an intrinsic connection between the cosmic microwave background (CMB) formed by the primordial perturbation of the early universe and the large-scale structure of the universe observed today; therefore, we can conclude that there is also a relationship between the γ-ray from the PBHs and the CMB lensing signal. In this letter, we use the cross-correlation technique, which has been widely used as a sophisticated DM indirect detection method by many previous works (Ando 2014; Cuoco et al. 2015; Fornengo et al. 2015; Regis et al. 2015; Xia et al. 2015; Branchini et al. 2017;

Cuoco et al. 2017; Tan et al. 2020, 2020), to search for this kind of connection by simulating the future e-ASTROGAM and CMB-S4 (CMB-S4 Collaboration et al. 2014) projects and constrain the PBH fraction.

2. Window Function

The γ-ray emissions in the MeV range produced by PBHs could trace the density field. Therefore, we have the source field of PBHs, which provides a primordial seed for the specific observable along the line-of-sight direction, $\hat{\mathbf{n}}$ $g_{\rm PBH}(\chi, \hat{\boldsymbol{n}}) = \rho_{\rm PBH}(\chi, \hat{\boldsymbol{n}})$. Inspired by the expression of intensity from Arbey et al. (2020, and references therein), we could define the window function of PBHs as

$$W_{\rm PBH}(\chi) = \frac{f_{\rm PBH}\,\Omega_{\rm DM}\rho_c}{4\pi M_{\rm PBH}} \times \int_{\delta E}\int_{t_{\rm min}}^{t_{\rm max}} \left[\frac{d^2N}{dtdE_\gamma}\right]_{\rm tot} E_\gamma(\chi) e^{-\tau[\chi, E_\gamma(\chi)]} dE_\gamma dt, \quad (1)$$

where $d^2N/dtdE_\gamma$ denotes the number of particles N emitted per units of energy and time, $\chi = \chi(z)$ represents the comoving distance, $\tau[\chi, E_\gamma(\chi)]$ is the optical depth, and the time integral runs from $t_{\rm min} = 380{,}000$ yr at last scattering of the CMB to $t_{\rm max} = \min(t(M), t_0)$, where $t(M)$ is the PBH lifetime with mass M, and t_0 is the age of the universe.

In the theory of Kerr PBHs, the number density of photons from an evaporating PBH, depending on the PBH's mass $M_{\rm PBH}$ and the dimensionless spin parameter $a_* \equiv J/GM_{\rm PBH}^2 \in [0, 1]$ (J is the PBH's angular momentum), in a certain energy range and time interval, $\left[\frac{d^2N}{dtdE_\gamma}\right]_{\rm pri} = \frac{1}{2\pi}\sum_{\rm dof}\frac{\Gamma^j}{\exp[E'/T_{\rm PBH}] - (-1)^{2s}}$, where Γ is the graybody factor for each particle species, $E' = E - \frac{m}{2M}\frac{a_*}{1+\sqrt{1-a_*^2}}$ is the total energy of the particle, j indicates particle species, s refers to the spin of the particle, and $T_{\rm PBH}$ is the temperature from radiation of PBHs. When $a_* = 0$, this reverts to the standard Schwarzschild PBHs. If a_* is close to unity, the spin of the PBHs will approach the maximum, and the temperature can change by orders of magnitude. The PBHs formed during radiation time tend to have low spin with $a \lesssim 0.4$ according to a theoretical prediction from Chiba & Yokoyama (2017). The probability of extreme-spin PBHs is low, according to Chongchitnan & Silk (2021); thus, we mainly focus on the $a_* = 0$ case and give a mild $a_* = 0.5$ and an extreme spin $a_* = 0.9999$ for comparison.

The total photon spectrum is combined by the primary component from the direct HE, which is a graybody factor counting the probability that a Hawking particle evades the PBH gravitational well, and the secondary emission from HE, which is generated from the hadronization and decays. In our calculations, we use the public software `BlackHwak` (Arbey & Auffinger 2019, 2021) to generate the photon spectra with three spin conditions, $a_* = \{0, 0.5, 0.9999\}$. In Figure 1, we illustrate the primary photon spectra of different mass ($M_{\rm PBH} \in [10^{15}, 5 \times 10^{18}]$ g) for the standard Schwarzschild PBHs, and the maximum of the total photon spectra is around the MeV energy band for the PBH mass range 10^{16}–5×10^{18} g. We are only using primary photon spectra to settle down the peak energy of the contribution from PBHs, since the secondary spectra could pull peaks out of the main energy range in our consideration. At the end, we added both of the spectra to estimate the flux.

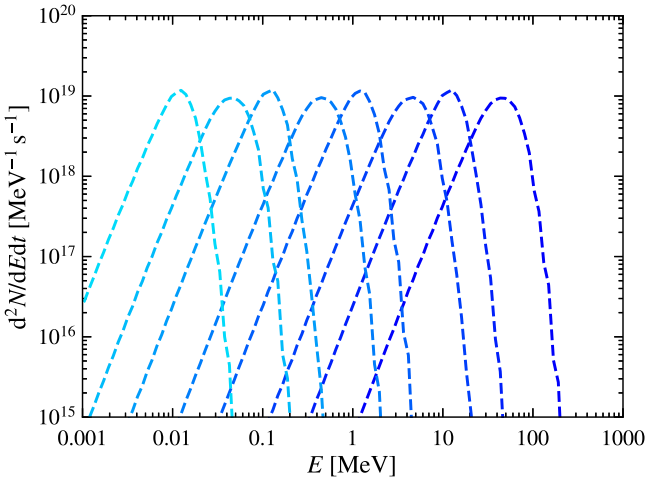

Figure 1. Primary photon spectra $d^2N/dtdE_\gamma$ of different $M_{\rm PBH}$ from 10^{15} to 5×10^{18} g with the spin $a_* = 0$, calculated by `BlackHwak`. The larger the mass of the PBHs is, the lighter the color of the line becomes. From left to right, the lines denote the masses of PBHs: 5×10^{18}, 1×10^{18}, 5×10^{17}, 1×10^{17}, 5×10^{16}, 1×10^{16}, 5×10^{15}, and 1×10^{15}.

The CMB lensing convergence, κ, in a given line of sight is the integral over all of the matter fluctuations that will cause gravitational lensing, $\kappa(\hat{\boldsymbol{n}}) = \int dz W_\kappa(z)\delta(\chi\hat{\boldsymbol{n}}, z)$, where $\delta(\chi\hat{\boldsymbol{n}}, z)$ is the overdensity of matter at a comoving distance χ and redshift z. The distance kernel is given by

$$W_\kappa(z) = \frac{3}{2}\Omega_{\rm m}H_0^2\frac{1+z}{H(z)}\frac{\chi(z)}{c}\left[\frac{\chi_{\rm CMB} - \chi(z)}{\chi_{\rm CMB}}\right], \quad (2)$$

where $\Omega_{\rm m}$ is the fraction of the matter density today compared to the present critical density of the universe, H_0 is the Hubble parameter today, $H(z)$ is the Hubble parameter as a function of redshift, c is the speed of light, and $\chi_{\rm CMB}$ is the comoving distance to the surface of last scattering where the CMB was emitted.

As the γ-ray emission intensity from PBHs is expected to be biased tracers of matter fluctuations, we can use the Limber approximation (Limber 1954) to write the cross-correlation power spectrum between γ-ray emission intensity from PBHs and CMB lensing,

$$C_\ell^{\kappa,\rm PBH} = \int\frac{dz}{c}\frac{H(z)}{\chi^2(z)}W_\kappa(z)W_{\rm PBH}(z)P_{\kappa,\rm PBH}(k = \ell/\chi, z), \quad (3)$$

where $P_{\kappa,\rm PBH}$ is the 3D power spectrum of cross-correlation between CMB lensing and the γ-ray emissions from PBHs, which consists of two parts in the halo model, $P_{\kappa,\rm PBH} = P_{\kappa,\rm PBH}^{\rm 1h} + P_{\kappa,\rm PBH}^{\rm 2h}$, and the mass integral runs from $M_{\rm min} = 10^7$ to $M_{\rm max} = 10^{18}\,M_\odot$. For the halo bias of PBHs, we directly take from Equation (12) of Sheth & Tormen (1999). Furthermore, we include the contribution from the isocurvature perturbation to the linear part whose detailed description and the halo mass function of PBHs is following Gong & Kitajima (2017).

3. Astrophysical Sources

Besides the PBH emission by the HE, AGNs, galaxies and clusters can also provide significant contributions to the γ-ray emission of the sky in the MeV energy range. Among these three astrophysical sources, the clusters of galaxies can emit

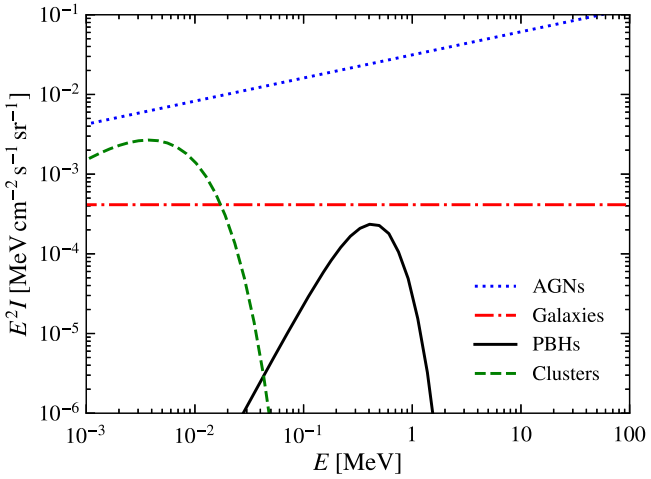

Figure 2. Total intensity produced by AGNs (blue dotted line), galaxies (red dashed–dotted line), and the cluster of galaxies (green dashed line). For comparison, we also plot the PBH emission (black solid line) with $M_{\rm PBH} = 10^{17}$ g, the spin $a_* = 0$, and the fraction $f_{\rm PBH} = 10^{-3}$.

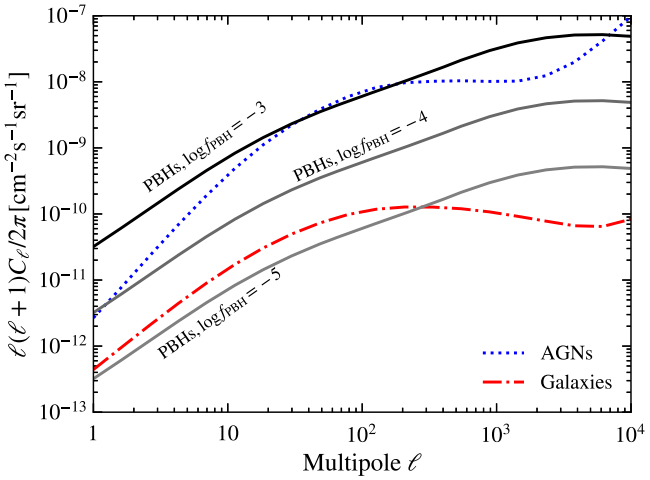

Figure 3. Cross-correlation angular power spectra between the CMB lensing and AGNs (blue dotted line), galaxies (red dashed–dotted line), and PBHs (black solid lines). Here we choose the PBH mass $M_{\rm PBH} = 10^{17}$ g and the spin $a_* = 0$. From top to bottom, we show power spectra from different values of the PBH fraction: $f_{\rm PBH} = 10^{-3}$, 10^{-4}, and 10^{-5}.

high-energy emissions by means of bremsstrahlung radiation of their gas. We calculated the intensity from bremsstrahlung radiation according to Zandanel et al. (2015) and found that the main contribution of the clusters appears in the energy band <40 keV, which is not covered by the energy range of the e-ASTROGAM project. Therefore, in the following calculations, we neglect the contribution from the clusters.

Following Ptak et al. (2007), Aird et al. (2010), and Caputo et al. (2020), we could obtain the window functions $W(z)$ of AGNs and galaxies,

$$W_{\rm X}(E, z) = \int_{L_{\rm X,min}}^{L_{\rm X,max}(F_{\rm sens}, z)} \frac{dL_{\rm X}}{L_{\rm X}} \Phi_{\rm X}(L_{\rm X}, z)\mathcal{L}_{\rm X}(E, z), \qquad (4)$$

where $\Phi_{\rm X}(E, z)$ denotes the differential luminosity at an energy E (defined as a number of photons emitted per unit time and per unit energy range; the subscript X refers to AGNs or galaxies) at redshift z. We set the minimal luminosity $L_{\rm X,min} = 10^{39}$ erg s^{-1}, while the maximum luminosity $L_{\rm X,max}$ of an unresolved source is dictated by the sensitivity flux $F_{\rm sens}$ of the γ-ray experiment, providing the minimum detectable flux. The intensity provided by the astrophysical emitters is reported in Figure 2, where we compare the prediction from the intensity of PBHs.

Similar to Equation (3), we can also obtain the cross-correlation signals between the CMB lensing and two astrophysical sources, which are shown in Figure 3. Obviously, the power spectrum of AGNs contributes most of the signal, while the signal from galaxies is much smaller and mainly on large scales. Here we also illustrate the signals from PBHs with different fraction values to demonstrate their effects on the cross-correlation power spectrum signal. From the black curves in the figure, we can see that the amplitude of the power spectrum signal is highly dependent on the PBH fraction, since numerous PBHs will significantly enhance the cross-correlation signal between the CMB lensing and PBHs. The signal from PBHs will be comparable to that from AGNs when $f_{\rm PBH} = 10^{-3}$.

3.1. Future Experiments

The e-ASTROGAM observatory (e-ASTROGAM et al. 2018) is dedicated to the study of the nonthermal universe in the photon range from 0.15 MeV to 3 GeV by carrying a γ-ray telescope. In this work, we estimate the capability of an instrument with the sensitivity of the e-ASTROGAM to explore the ability of constraints on the PBH fraction. We adopted the effective area, angular resolution, and flux sensitivity varied in energy intervals according to Tables 3 and 4 of e-ASTROGAM et al. (2017); the angular selection is shown in Table 1 for different masses of PBHs. We take the observational time of 10^6 s and focus on a fraction of sky $f_{\rm sky} = 0.23$, corresponding to a field of view $\Omega = 2.9$ sr. The flux sensitivity is 1.1×10^{-12} erg cm^{-1} s^{-1} for all energy ranges, and the particle background is 1.4 counts s^{-1} sr^{-1} in calculation.

As we show in Figure 1, the photon spectra as a function of the energy band have peaks at different energies for different masses of PBHs. Correspondingly, we list the peak energy $E_{\rm peak}$ for different $M_{\rm PBH}$ with three values of spin in Table 1. Apparently, the larger the mass of the PBHs is, the lower energy peak it has. We notice that when considering the mass of PBHs $M_{\rm PBH} > 5 \times 10^{17}$ g, the peak energy $E_{\rm peak}$ is already out of the energy range of e-ASTROGAM. Therefore, for these masses of PBHs, we did not consider photons near the peak energy (see Table 1) but rather only photons within the lowest energy band of the energy range of e-ASTROGAM, i.e., from 150 to 300 keV.

For CMB lensing, we assume a CMB-S4 experiment (CMB-S4 Collaboration et al. 2014) with a telescope beam of FWHM $= 1'$ and a white-noise level of 1 $\mu K'$ for temperature and 1.4 $\mu K'$ for polarization. We set the noise levels $N_\ell^{\rm TT}$ and $N_\ell^{\rm EE}$ in the primary CMB as Gaussian noise as $N_\ell^{\rm XX} = s^2 \exp\left(\ell(\ell+1)\frac{\theta^2_{\rm FWHM}}{8\log 2}\right)$, where XX stands for TT or EE; here s is the total intensity of instrumental noise in μK rad, and $\theta^2_{\rm FWHM}$ is the FWHM of the beam in radians. For the CMB lensing reconstruction noise, we use the EB quadratic estimator method described in Hu & Okamoto (2002), implemented by the `QUICKLENS` software package.[4]

[4] https://github.com/dhanson/quicklens/

Table 1
The Best Energy Performance $E_{\rm peak}$ (keV) and Angular Resolution σ_b Selection Used for Different Masses of PBHs

$M_{\rm PBH}$ (g)	1×10^{16}	3×10^{16}	5×10^{16}	7×10^{16}	1×10^{17}	3×10^{17}	5×10^{17}	7×10^{17}	1×10^{18}	3×10^{18}	5×10^{18}
$a_*=0$	4690	2234	1204	831	448	213	150	102	50	23	12
$a_*=0.5$	4690	2234	1362	940	507	213	150	102	50	23	12
$a_*=0.9999$	7690	3662	2234	1541	831	350	213	167	79	38	20
σ_b	0.°8	0.°8	1.°1	1.°5	1.°5	2.°5	4.°3	4.°3	4.°3	4.°3	4.°3

Finally, we compute the theoretical power spectra and perform the numerical constraint on the PBH fraction. The redshift range we consider is from zero to 10, which is reasonable for both PBHs and the astrophysical sources. Furthermore, we assume a flat ΛCDM cosmology with parameters set by Planck results (Aghanim et al. 2020): $h=0.6766$, $\Omega_{\rm b}h^2=0.02243$, $\Omega_{\rm c}h^2=0.11999$, $\tau=0.0561$, and $n_s=0.9665$.

4. Constraint Results

Assuming the experiments are the power spectra of Gaussian random fields, we can compute the covariance matrix as

$$\Gamma^{\gamma,\kappa}_{\ell,\ell'}=\frac{\delta_{\ell\ell'}}{(2\ell+1)f_{\rm sky}\,\Delta\ell}\times[C^{\gamma\kappa}_{\ell}C^{\gamma\kappa}_{\ell'}+(C^{\gamma}_{\mathcal{N}}+\sqrt{C^{\gamma}_{\ell}C^{\gamma}_{\ell'}})(C^{\kappa}_{\mathcal{N}}+C^{\kappa}_{\ell})],\qquad(5)$$

where the photon noise term above is $C^{\gamma}_{\mathcal{N}}=4\pi f_{\rm sky}\langle I_{\rm X}\rangle^2 N_{\rm X}^{-1}W_{\ell}^{-2}$, and $\langle I_{\rm X}\rangle$ refers to the sky-averaged intensity observed by the telescope and is assumed to come from the AGN and galaxy contributions by default; $N_{\rm X}=\langle I_{\rm X}A_{\rm eff}\rangle t_{\rm obs}\Omega_{\rm FoV}$; the beam window $W_{\ell}=\exp(-\sigma_{\rm b}^2\ell^2/2)$ is a Gaussian point-spread function, where $\sigma_{\rm b}$ is the angular resolution of the instrument, which is described in Section 3.1 and adopted to Table 3 from e-ASTROGAM et al. (2018); and Table 1 gives the values for every mass of PBHs.

The upper limits on the parameter space of the PBH fraction are derived at a 95% confidence level (C.L.) by requiring $\chi^2=2.71$ with the estimator assumed to follow a χ^2 distribution with one degree of freedom, which is $\chi^2=\sum_{\ell}(C^{\gamma,\kappa}_{\ell}\Gamma^{-1}_{\ell\ell'}C^{\gamma,\kappa}_{\ell'})$, where the sum of the multipoles is from $\ell_{\rm min}=10$ to $\ell_{\rm max}=500$, which is corresponding to the angular scale 0.°36. Since the angular resolution σ_b used in Equation (5) is larger than 0.°8, in practice, we find that the photon shot-noise term will dramatically increase at high multipoles. Therefore, this choice of $\ell_{\rm max}$ basically does not affect the final results. It is worth noting that only the cross-correlation term involving the PBHs is present in the signal part of χ^2 the function, since we assume to be able to extract the background associated with the emitting AGNs and galaxies to a good precision and neglect model uncertainties in the astrophysical components. Furthermore, we do not sum up the energy bins, since for each mass of PBHs, the energy range for integration will be around the different $E_{\rm peak}$ as we mentioned before.

In Figure 4, we present the 95% C.L. constraints on the PBH fraction for different $M_{\rm PBH}$. The blue solid line is our main result for the standard Schwarzschild PBHs. The limit on $f_{\rm PBH}$ is around 10^{-5} for $M_{\rm PBH}=10^{16}$ g and down to 10^{-3} when increasing the mass of PBHs to 10^{17} g. The cross-correlation between γ-ray emissions and CMB lensing significantly compresses the allowed space of $f_{\rm PBH}$ for low-mass PBHs. This constraint is much tighter than the limits on

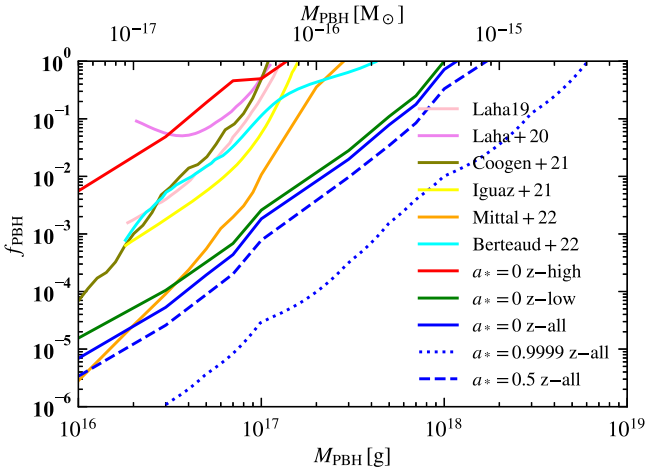

Figure 4. The 95% C.L. bounds on the PBH fraction as a function of the PBH masses when considering different cases. See text for details.

$f_{\rm PBH}$ from other observations[5] by about 2 orders of magnitude, such as the result based on Comptel observations of the central region of the galaxy (olive line; Coogan et al. 2021), as well as the recent limitation from the 21 cm absorption signal of the EDGES experiment (orange line) at $M_{\rm PBH}>10^{17}$ g (Mittal et al. 2022). We also exhibit the outputs from some important PBH works for comparison: the Galactic center 511 keV line (Laha 2019; pink line), the published spectrometer on board the INTEGRAL satellite (SPI) results (Laha et al. 2020; purple line), using the cosmic X-ray background (Iguaz et al. 2021; yellow line), and from diffuse soft γ-ray emission toward the inner galaxy as measured by the SPI data (Berteaud et al. 2022; cyan line).

The reason for this tight constraint is the flux sensitivity of e-ASTROGAM, which is also the key parameter for the photon noise term. Because of the low sensitivity, the sky-averaged intensity observed by the telescope $\langle I_{\rm X}\rangle$ will be significantly larger than that when using other experiments with high sensitivity, like the Athena project (Nandra et al. 2013). This will suppress the shot-noise term in the covariance matrix of Equation (5) and improve the constraints on $f_{\rm PBH}$.

5. Conclusions and Discussions

In the calculations above, we consider the cross-correlation signal in the redshift range [0, 10] (z-all), which gives very tight constraints on the PBH fraction for the PBH mass range $[10^{16}, 10^{18}]$ g. In order to investigate the constraining power on the PBH fraction further, we split the redshift range into two other ranges for integration: [0, 1] (z-low) and [1, 10] (z-high). The reason for separating these three bins is to roughly determine the majority redshift region of PBHs that can be

[5] https://github.com/bradkav/PBHbounds/

distinguished from astrophysical sources. In Figure 4, we also show the constraints on $f_{\rm PBH}$ for the z-low (green solid line) and z-high (red solid line) cases. If we only take the low-redshift information with the z-low case into account, we obtain that the limitation on $f_{\rm PBH}$ is slightly tighter than the z-all case, which means that the constraining power for PBHs can be more visible in the low-redshift universe. For the z-high case, since we discard the low-redshift information, the constraining power on $f_{\rm PBH}$ becomes very weak. If we use the z-all, which includes both the low- and high-redshift information, the constraint on the PBH fraction becomes an averaged consequence of them.

All of the above conclusions are calculated in the standard Schwarzschild case $a_* = 0$. In fact, we also computed the photon spectra with three different spins. When we consider the PBHs with high rotation, the cross-correlation signal with CMB lensing will be significantly enlarged. Consequently, the constraints on the PBH fraction will be improved in the high-rotating PBHs. In Figure 4, we also showed the limits of $f_{\rm PBH}$ as a function of $M_{\rm PBH}$ for different spins: $a_* = 0.5$ (blue dashed line) and $a_* = 0.9999$ (blue dotted line). For the $a_* = 0.5$ case, the constraints are only slightly enhanced, while in the $a_* = 0.9999$ case, the limitation on $f_{\rm PBH}$ becomes significantly improved by more than an order of magnitude. The 95% C.L. limitation on the PBH fraction is around 10^{-2} at about $M_{\rm PBH} = 10^{18}$ g. And the limitation will be close to 1 until the PBH mass $M_{\rm PBH}$ is larger than $\sim 2 \times 10^{18}$ g. This cross-correlation analysis could importantly fill the gaps with PBH fraction limits in the mass range 5×10^{17}–2×10^{18} g.

Finally, we conclude that based on future projects, like e-ASTROGAM and CMB-S4, we obtain very tight limitations on the fraction of the Schwarzschild PBHs in the mass range 10^{16}–5×10^{17} g. The constraining ability of the spin PBH fraction can be improved by more than 1 order of magnitude, which could importantly fill gaps in PBH fraction limits in the mass range 5×10^{17}–2×10^{18} g.

We thank Marco Regis and Marco Taoso for useful suggestions on the calculations. J.-Q.X. is supported by the National Science Foundation of China under grant Nos. U1931202 and 12021003 and the National Key Research and Development Program of China under grant No. 2020YFC2201603. T.Q. is supported by the National Science Foundation of China under grant No. 11875141 and the National Key Research and Development Program of China under grant No. 2021YFC2203100.

References

Aghanim, N., Akrami, Y., Ashdown, M., et al. 2020, A&A, 641, A6
Aird, J., Nandra, K., Laird, E. S., et al. 2010, MNRAS, 401, 2531
Ando, S. 2014, JCAP, 10, 061
Arbey, A., & Auffinger, J. 2019, EPJC, 79, 693
Arbey, A., & Auffinger, J. 2021, EPJC, 81, 10
Arbey, A., Auffinger, J., & Silk, J. 2020, PhRvD, 101, 023010
Auffinger, J. 2022, EPJC, 82, 384
Ballesteros, G., Coronado-Blázquez, J., & Gaggero, D. 2020, PhLB, 808, 135624
Berteaud, J., Calore, F., Iguaz, J., Serpico, P. D., & Siegert, T. 2022, PhRvD, 106, 023030
Boveia, A., & Doglioni, C. 2018, ARNPS, 68, 429
Branchini, E., Camera, S., Cuoco, A., et al. 2017, ApJS, 228, 8
Caputo, A., Regis, M., & Taoso, M. 2020, JCAP, 03, 001
Carr, B., Kohri, K., Sendouda, Y., & Yokoyama, J. 2021, RPPh, 84, 116902
Carr, B., Kuhnel, F., & Sandstad, M. 2016, PhRvD, 94, 083504
Carr, B. J., Kohri, K., Sendouda, Y., & Yokoyama, J. 2010, PhRvD, 81, 104019
Chiba, T., & Yokoyama, S. 2017, PTEP, 2017, 083E01
Chongchitnan, S., & Silk, J. 2021, PhRvD, 104, 083018
CMB-S4 Collaboration, Abazajian, K. N., Adshead, P., et al. 2014, arXiv:1610.02743
Coogan, A., Morrison, L., & Profumo, S. 2021, PhRvL, 126, 171101
Cuoco, A., Bilicki, M., Xia, J.-Q., & Branchini, E. 2017, ApJS, 232, 10
Cuoco, A., Xia, J.-Q., Regis, M., et al. 2015, ApJS, 221, 29
DeRocco, W., & Graham, P. W. 2019, PhRvL, 123, 251102
e-ASTROGAM, De Angelis, A., Tatischef, V., et al. 2017, ExA, 44, 25
e-ASTROGAM, De Angelis, A., Tatischeff, V., et al. 2018, JHEAp, 19, 1
e-ASTROGAM, Tatischeff, V., De Angelis, A., et al. 2018, Proc. SPIE, 10699, 106992J
Fornengo, N., Perotto, L., Regis, M., & Camera, S. 2015, ApJL, 802, L1
Gong, J. O., & Kitajima, N. 2017, JCAP, 08, 017
Hawking, S. 1971, MNRAS, 152, 75
Hawking, S. W. 1975, CMaPh, 43, 199
Hu, W., & Okamoto, T. 2002, ApJ, 574, 566
Iguaz, J., Serpico, P. D., & Siegert, T. 2021, PhRvD, 103, 103025
Laha, R. 2019, PhRvL, 123, 251101
Laha, R., Munoz, J. B., & Slatyer, T. R. 2020, PhRvD, 101, 123514
LIGO Scientific,Virgo Collaborations, Abbott, B. P. 2016, PhRvL, 116, 061102
Limber, D. N. 1954, ApJ, 119, 655
MacGibbon, J. H., Carr, B. J., & Page, D. N. 2008, PhRvD, 78, 064043
McEnery, J., van der Horst, A., Dominguez, A., et al. 2019, BAAS, 51, 245
Mittal, S., Ray, A., Kulkarni, G., & Dasgupta, B. 2022, JCAP, 03, 030
Nandra, K., Barret, D., Barcons, X., et al. 2013, arXiv:1306.2307
Pardo, K., & Spergel, D. N. 2020, PhRvL, 125, 211101
Ptak, A., Mobasher, B., Hornschemeier, A., Bauer, F., & Norman, C. 2007, ApJ, 667, 826
Ray, A., Laha, R., Munoz, J. B., & Caputo, R. 2021, PhRvD, 104, 023516
Regis, M., Xia, J.-Q., Cuoco, A., et al. 2015, PhRvL, 114, 241301
Saha, A. K., & Laha, R. 2022, PhRvD, 105, 103026
Sheth, R. K., & Tormen, G. 1999, MNRAS, 308, 119
Tan, X., Colavincenzo, M., & Ammazzalorso, S. 2020, MNRAS, 495, 114
Tan, X.-H., Dai, J.-P., & Xia, J.-Q. 2020, PDU, 29, 100585
Xia, J.-Q., Cuoco, A., Branchini, E., & Viel, M. 2015, ApJS, 217, 15
Zandanel, F., Weniger, C., & Ando, S. 2015, JCAP, 09, 060